JOURNAL OF MATERIALS SCIENCE **34** (1999) 3795–3800

Effect of ZrO_2 and SiO_2 on glass forming ability of $Zr_{57}Cu_{20}Al_{10}Ni_8Ti_5$ alloy

L. Q. XING, D. M. HERLACH
Institut für Raumsimulation, DLR, D-51170 Köln, Germany
E-mail: lqxing@hotmail.com

$Zr_{57}Cu_{20}Al_{10}Ni_8Ti_5$ has very high glass forming ability (GFA) due to its low crystal growth rate which limits development of crystallites arising from container walls or nuclei. Effect of ZrO_2 and SiO_2 on GFA was studied by investigating the solidification microstructures of alloys containing different amount of the oxides. Amorphous ingots were formed by melting and freezing alloys without addition of the oxides using an arc furnace. Partially amorphous ingots were formed for addition of the oxides up to 0.2 wt%. Amorphous forming conditions of alloys containing greater concentration of the oxides were studied using a drop tube. GFA decreases with increasing concentration of the oxides. However, superheating of melts eliminates some effects of the oxides. Different types of oxides leads to different microstructures due to their different heterogeneous nucleation rates and nucleation temperature.

1. Introduction

Heterogeneous nucleation agents affect glass forming ability (GFA) of alloys [1–4]. To decrease the critical cooling rate for glass formation or to increase the dimensions of amorphous samples prepared, various methods have been used to eliminate heterogeneous nucleation. Using thermal cycling and surface etching to remove the surface heterogeneous agents, Drehman *et al*. prepared bulk $Pd_{40}Ni_{40}P_{20}$ amorphous alloys with diameters up to 5.3 mm [5]. Kui *et al*. increased the dimensions of $Pd_{40}Ni_{40}P_{20}$ amorphous alloy up to 10 mm by using B_2O_3 as a flux [6]. Recently, He *et al*. prepared bulk $Pd_{40}Ni_{40}P_{20}$ amorphous rods of 25 mm diameter by water quenching following fluxing with B_2O_3 [7]. Xing *et al*. increased the critical dimensions for amorphous formation of $Ni_{75}B_{17}Si_8$ by fluxing with B_2O_3 and cyclically heating before quenching into a copper mould [8]. Gillessen *et al*. formed Cu-Zr amorphous droplets by using a drop tube to eliminate the container-wall-induced heterogeneous nucleation and compared the influence of melting conditions [9]. Kim *et al*. used levitation melting and containerless solidification to decrease the critical cooling rate for glass formation of $Zr_{41.2}Ti_{13.8}Cu_{12.5}Ni_{10}Be_{22.5}$ [10]. These previous studies aimed to purify the alloys as much as possible. However, for industrial applications of metallic glasses, alloys of high purity are too expensive and it is difficult to eliminate heterogeneous nucleation for mass production. In this work, we aimed to investigate the glass forming behaviour of alloys containing various amounts of heterogeneous nucleating agents, and the effects of eliminating heterogeneous nucleation by superheating the melt, which is the most practical way for industrial production. Recently, several alloys were found to have very high GFA, for example, Zr-Cu-Ni-Al [11], Zr-Ti-Cu-Ni-Be [12] and Zr-Ti-Al-Cu-Ni [13–15]. Experiments using these alloys may provide distinguish information because they permit addition of relatively large quantities of impurities and may form amorphous phases under a wide range of cooling rates. In the present experiment, $Zr_{57}Cu_{20}Al_{10}Ni_8Ti_5$ was used as sample alloy. ZrO_2 and SiO_2 were used as the added impurities in view of the fact that oxidation is the common source of contamination during melting and that quartz crucibles are usually used for melting.

2. Experimental

The "pure" $Zr_{57}Cu_{20}Al_{10}Ni_8Ti_5$ ingots was prepared by arc melting using components of the following purities: Zr 99.5%, Cu 99.99%, Ni 99.998, Al 99.999%, Ti 99.95%. In order to produce ingots containing various amounts of heterogeneous nucleating agents, different amounts of ZrO_2 and SiO_2 powders were wetted with ethyl alcohol and coated on the pieces of the components before arc melting. Amorphous specimens were prepared by remelting the alloys from the prepared ingots using an arc furnace and a drop-tube 8 m in length. For arc melting, the furnace was evacuated to 4×10^{-4} mbar and then filled with Ar (99.999% purity) to a pressure of 800 mbar. The sample mass was about 5 g. The melted sample had an ellipsoidal shape with axial lengths of about 12 mm by 10 mm. For the containerless solidification with the drop tube, the chamber was evacuated to 5×10^{-5} mbar and then filled with He (99.999% purity) to a pressure of 800 mbar. Alloys of mass about 1 g were melted in a quartz tube with a nozzle at the bottom, and then forced into the drop tube through the nozzle with Ar pressure. The structures of

the specimens were analyzed using X-ray diffraction, differential scanning calorimetry (DSC) and optical micrography. For the optical micrography, the specimens were etched using a solution of 40 ml $HNO_3 + 4$ ml $HF + 25$ g $CrO_3 + 70$ ml H_2O. The crystallization enthalpies of the amorphous samples were measured by integrating the areas of the crystallization peaks in the DSC traces. The amorphous fractions of the samples were estimated by comparing their crystallization enthalpy to that of the fully amorphous alloy.

3. Results and discussion

Melting and freezing the "pure" $Zr_{57}Cu_{20}Al_{10}Ni_8Ti_5$ alloy in the arc furnace results in formation of amorphous ingots, except for a thin crystalline layer on the bottom where the melt is in contact with the copper hearth. Fig. 1a shows a general view of the cross-section of an as-solidified ingot. On the bottom, there is a small dark coloured crystalline region (marked by an arrow and "B" in Fig. 1a). Fig. 1b shows the microstructures near the bottom of the ingot, indicating crystals growing from the bottom. There is a clear interface between the crystalline region and the amorphous region. The region with light contrast is amorphous (marked "C" in Fig. 1a). Fig. 1c shows an enlarged micrography of region C. Fig. 2 shows the X-ray diffraction pattern for the cross section after removing the bottom layer (marked "B" in Fig. 1a). The diffraction pattern shows no peaks for crystalline phases, indicating that this region is amorphous in the sense of X-ray diffraction examination. For DSC measurement, the specimen taken from the region "C" shows similar exothermic peaks to the amorphous alloys prepared by copper mould casting [16]. The crystallization enthalpy is 70 J/g, similar to that of the amorphous alloys cast with copper moulds [16].

The crystalline layer (Fig. 1a and b) is caused by heterogeneous nucleation due to the copper hearth. During cooling, the crystalline phase grows from the bottom interface upwards into the melt due to a temperature gradient; meanwhile, the melt in front of solidification

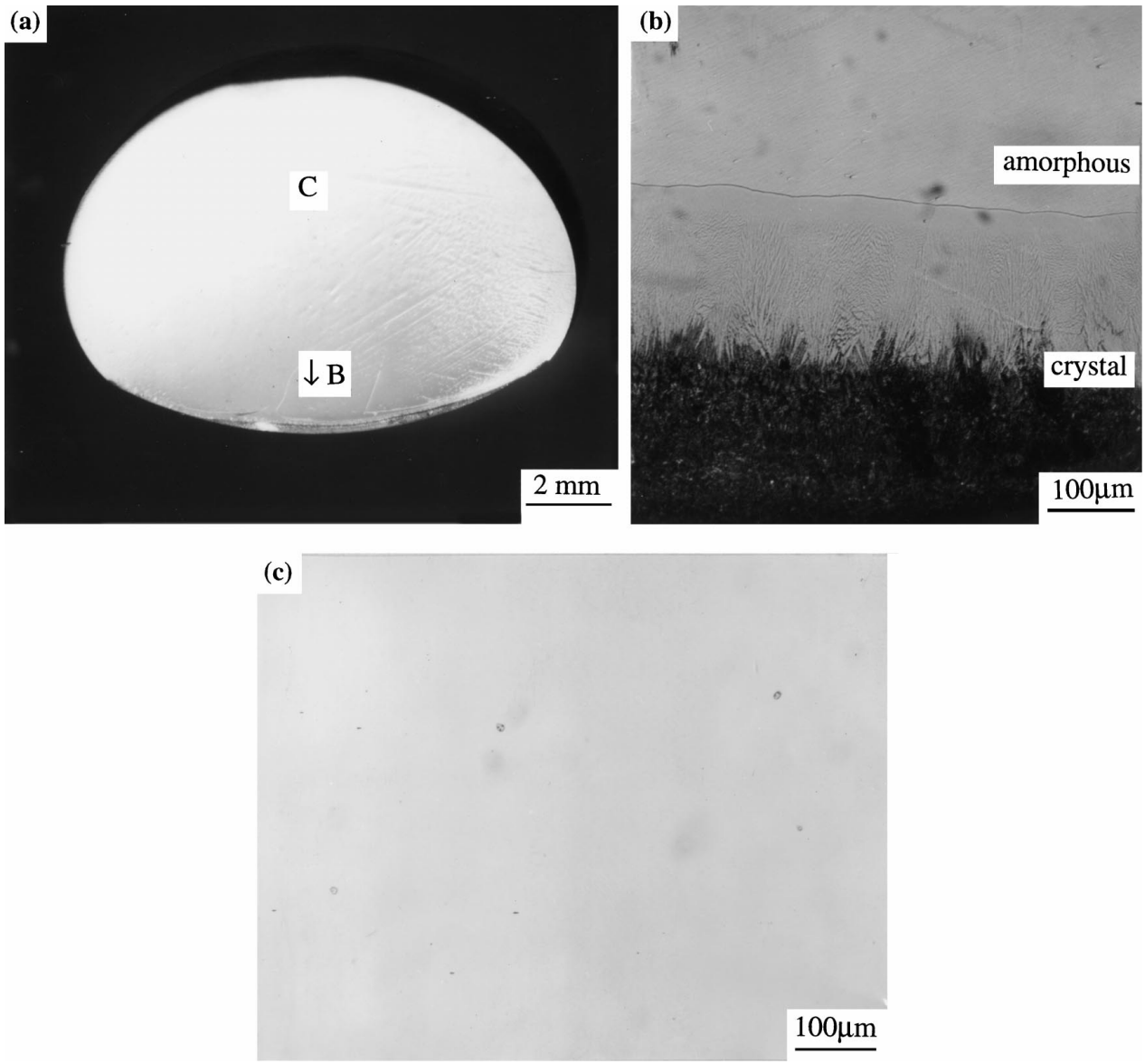

Figure 1 Glass forming conditions of $Zr_{57}Cu_{20}Al_{10}Ni_8Ti_5$ melted in an arc furnace. (a) General view of the cross-section of an ingot. (b) and (c) Microstructures near the bottom and in the center of the ingot (marked "B" and "C" in the micrograph (a) respectively).

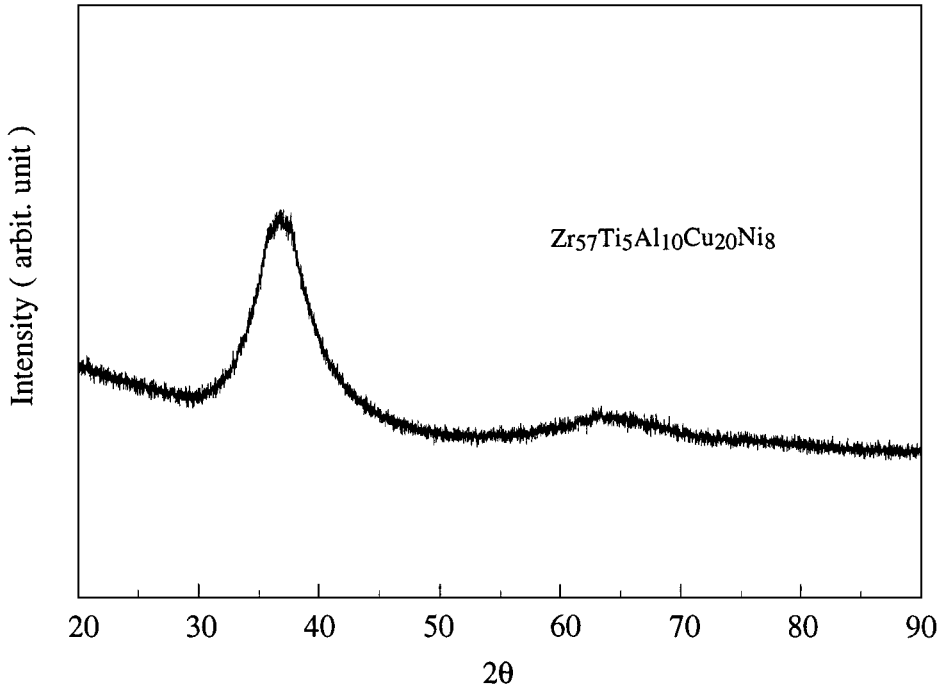

Figure 2 X-ray diffraction pattern of the ingot shown in Fig. 1 after removing the bottom crystalline layer.

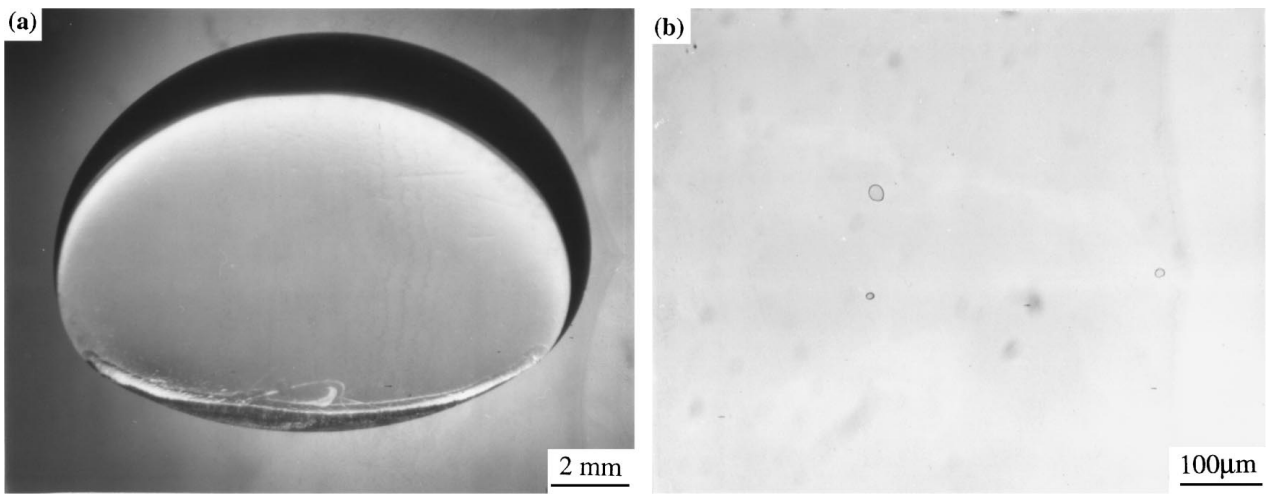

Figure 3 Glass forming conditions of $Zr_{57}Cu_{20}Al_{10}Ni_8Ti_5$ containing 0.05 wt % ZrO_2 by melting and freezing in an arc furnace. (a) General view of the cross-section of an ingot. (b) Microstructures in the central region of the ingot.

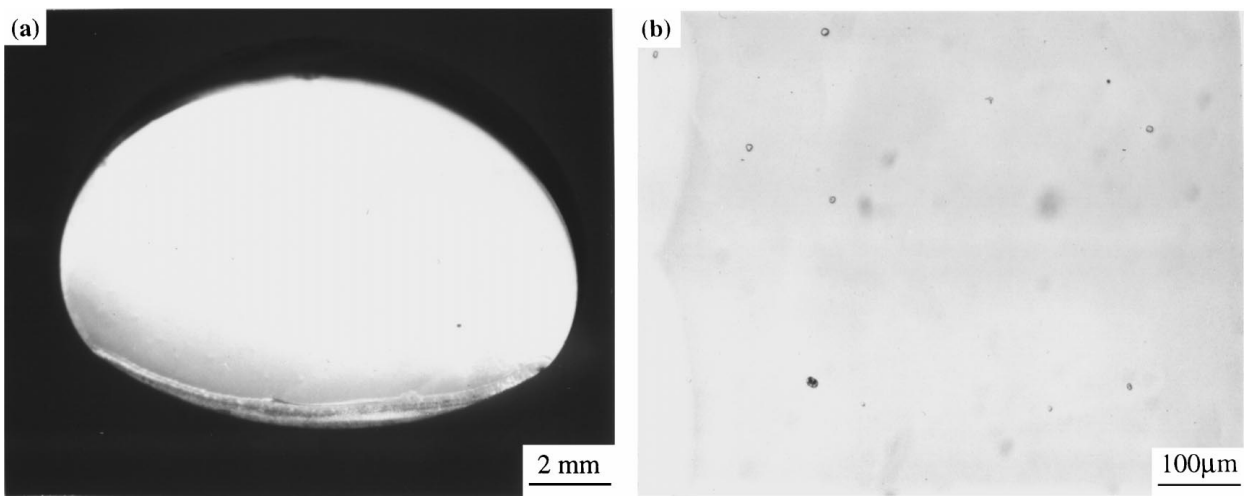

Figure 4 Glass forming conditions of $Zr_{57}Cu_{20}Al_{10}Ni_8Ti_5$ containing 0.05 wt % SiO_2 by melting and freezing in an arc furnace. (a) General view of the cross-section of an ingot. (b) Microstructures in the central region of the ingot.

interface undercools. When the melt in front of the solidification interface undercools close to the glass transition temperature, the crystal growth stops. The growing crystalline phase has a dendritic morphology (Fig. 1b). The crystalline layer grows only up about 0.5 mm during the cooling process, indicating that the crystal growth rate is very low. There are also some crystallites of diameters between about 2 μm and 10 μm precipitated in the amorphous matrix (Fig. 1c). These crystallites result from the presence of heterogeneous nuclei in the undercooled melt. We have investigated these microstructures by high resolution transmission microscopy (HRTEM). No nano-sized crystallites are present in the amorphous matrix, except for the micrometer-sized crystallites also seen by optical microscopy.

Samples containing 0.05 wt % ZrO_2 or SiO_2 were melted in the arc furnace two times for about one minute in each case. Fig. 3a shows the cross-section of a solidified ingot containing 0.05 wt % ZrO_2. Fig. 3b shows the microstructure in the center region of the ingot. Fig. 4a and b are the corresponding micrographs for an ingot containing 0.05 wt % SiO_2. The glass forming conditions for these two ingots are similar to that for the ingot shown in Fig. 1. The crystalline layers on the bottoms of these ingots are also of thickness about 0.5 mm. The number density of crystallites precipitated in the amorphous matrices (Figs 3b and 4b) are not significantly higher than that for the relatively pure alloy (Fig. 1b). It is supposed that the melts can dissolve some amount of the oxides when they are heated to very high temperature for some time. Therefore, overheating of melts for a period of time has the effect of eliminating a proportion of heterogeneous nuclei.

Alloys containing 0.2 wt % ZrO_2 or SiO_2 were melted by the same procedures as described above. Fig. 5a shows the cross-section of a solidified ingot containing 0.2 wt % ZrO_2. Fig. 5b and c are, respectively, microstructures of the regions marked "B" and "C" in Fig. 5a. Fig. 6a–c are the corresponding micrographs for the samples containing 0.2 wt % SiO_2. These ingots can be divided into three regions according to the glass forming conditions. One region is the crystalline layer on the bottom of the ingot (Figs 5a and 6a), which arises from the copper hearth. The second region is a mixture of amorphous and crystalline phase (marked "B" in Figs 5a and 6a). As shown in Fig. 5b, the mixed region for the alloy containing 0.2 wt % ZrO_2 has larger but fewer crystallites. In contrast, the mixed region for the ingot containing 0.2 wt % SiO_2 has larger number of much smaller crystallites. Measured on the basis of crystallization enthalpy, the amorphous fractions in the region with light contrast (marked "B" in Fig. 6a) are between 60 and 90%. The sizes of the precipitated crystallites can be related to the heterogeneous nucleation temperatures. ZrO_2 is supposed to have higher heterogeneous nucleation temperature but lower nucleation rate. In contrast, SiO_2 has lower heterogeneous nucleation temperature but higher nucleation rate. The third regions are marked "C" in Figs 5a and 6a. These regions are almost fully crystalline although the microstructures are different. The ingot containing

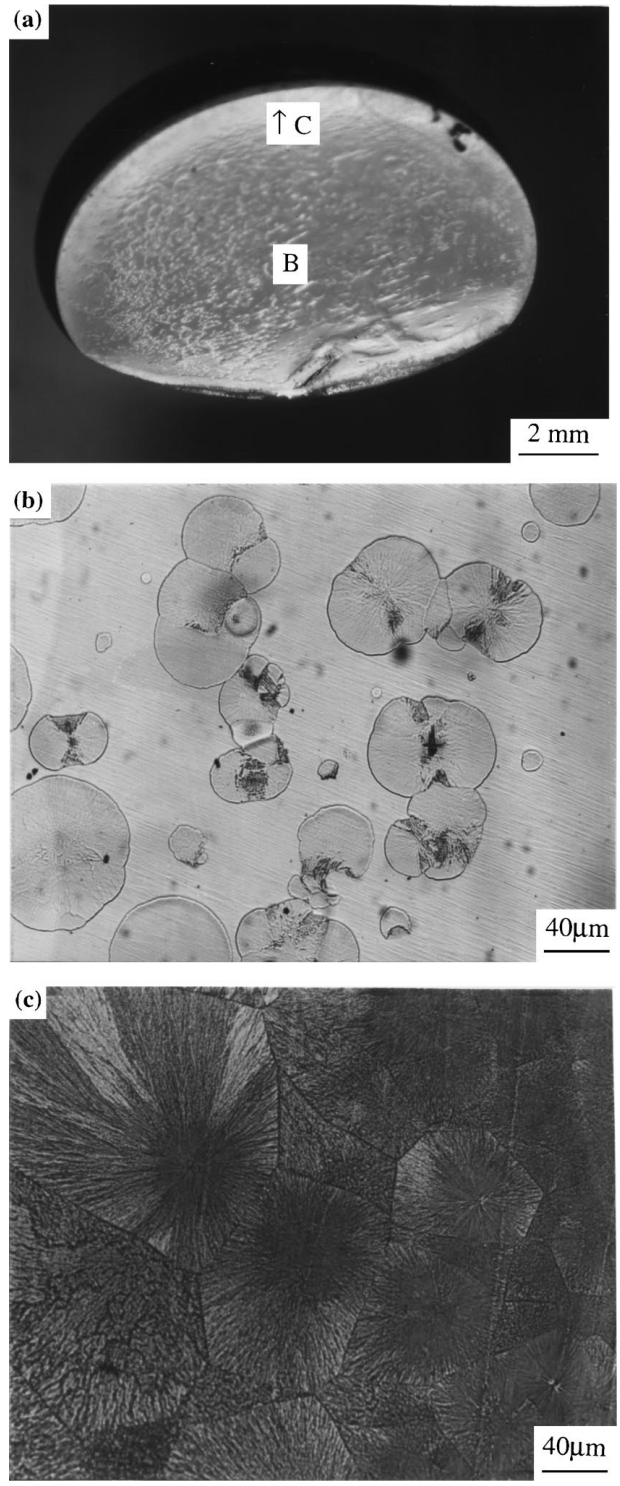

Figure 5 Glass forming conditions of $Zr_{57}Cu_{20}Al_{10}Ni_8Ti_5$ containing 0.2 wt % ZrO_2 by melting and freezing in an arc furnace. (a) General view of the cross-section of an ingot. (b) and (c) Microstructures corresponding to the regions marked "B" and "C" in the micrograph (a).

0.2 wt % ZrO_2 has much larger grains than that containing 0.2 wt % SiO_2. The area of fully crystalline region is larger for the ingot containing 0.2 wt % SiO_2 than for the ingot containing the 0.2 wt % ZrO_2. These results indicate that the solidification microstructures are dependent on the types and amounts of heterogeneous nuclei and on the cooling rate (or temperature gradient). Amorphous phase forms when the temperature gradient (cooling rate) is high enough to eliminate heterogeneous nucleation, for example in the case of

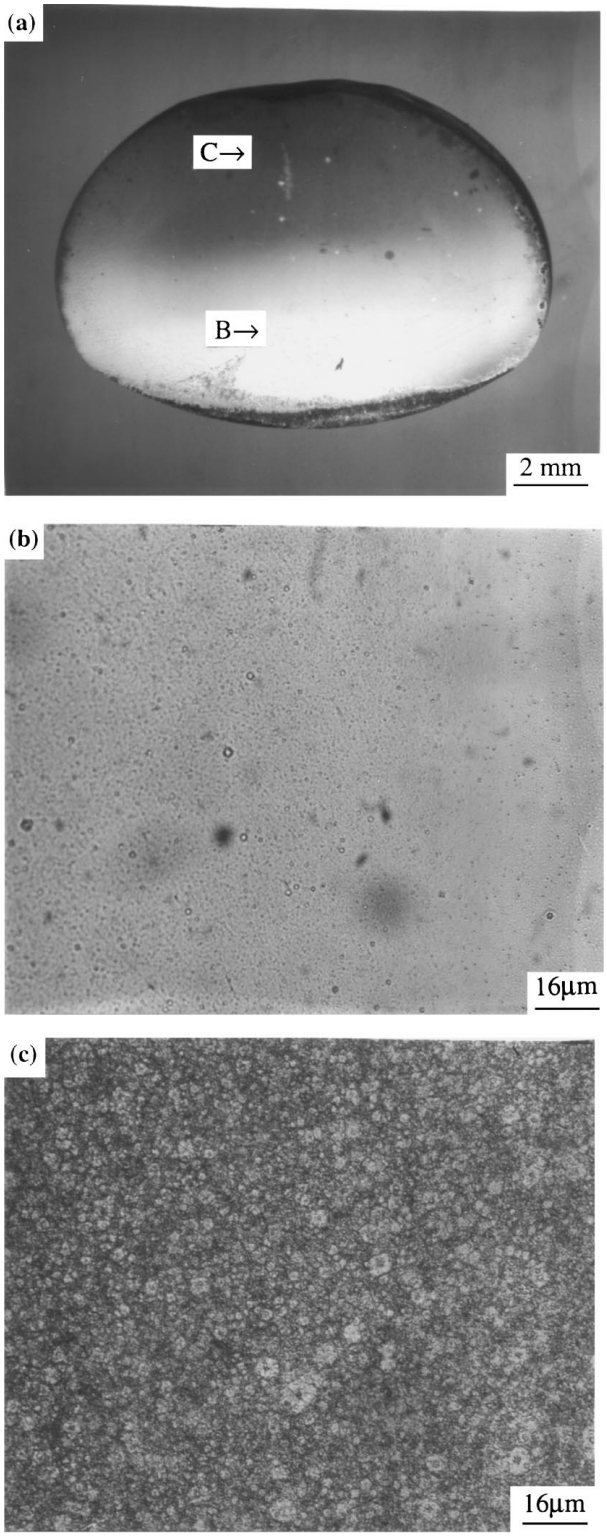

Figure 6 Glass forming conditions of $Zr_{57}Cu_{20}Al_{10}Ni_8Ti_5$ containing 0.2 wt % SiO_2 by melting and freezing in an arc furnace. (a) General view of the cross-section of an ingot. (b) and (c) Microstructures corresponding to the regions marked "B" and "C" in the micrograph (a).

Figs 1, 3 and 4. Under this condition, very small or no regions of mixed amorphous and crystalline phases appear, and the interface between the amorphous region and the crystalline region is very sharp in cases where a crystalline region arises from the container wall. For appropriate heterogeneous nucleation rates and temperature gradients, a region of mixed microstructures may form, as shown Figs 5 and 6. Accordingly, a fully

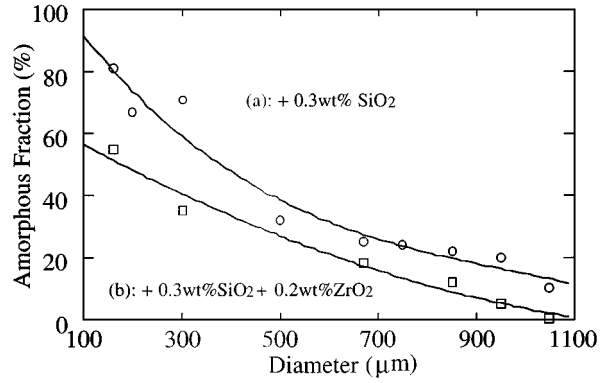

Figure 7 Amorphous fraction of $Zr_{57}Cu_{20}Al_{10}Ni_8Ti_5$ droplets solidified during the free fall in a drop tube as a function of the average droplet diameter. (a) Alloy with addition of 0.3 wt % SiO_2. (b) Alloy with addition of 0.3 wt % $SiO_2 + 0.2$ wt % ZrO_2.

crystalline region forms with further increase of the heterogeneous nucleation rate or decrease of the temperature gradient, e.g. in the upper region of the samples shown in Figs 5 and 6.

For the alloys with greater concentration of added oxides, the glass forming behaviour was investigated using the drop tube. The melting was performed at about 1370 K for about 1 minute. Droplets up to about 1000 μm in diameter solidified during the free fall and were collected at the bottom of the drop tube. The droplets were sized with assorted wire meshes. The droplets of each size group were analyzed with respect to their amorphous fractions by DSC (by comparing their crystallization enthalpy with that of the fully amorphous alloy). Fig. 7 shows the amorphous fractions of the droplets as a function of the average droplet diameters. Curve (a) is for the alloy containing 0.3 wt % SiO_2. Curve (b) is for the alloy containing 0.3 wt % $SiO_2 + 0.2$ wt % ZrO_2. These curves show that the amorphous fraction decreases as the weight fraction of the oxides is increased. In contrast to the results for a Zr-Cu alloy [9], a mixed microstructure of amorphous and crystalline phases forms over a very wide range of cooling rates for Zr-Ti-Cu-Ni-Al. The amorphous fraction decreases from 80 to 20% as the droplet diameter increases from about 200 μm to about 300 μm for the $Cu_{62}Zr_{38}$, and from 100 μm to about 200 μm for the $Cu_{56}Zr_{44}$ [9]. In contrast, the amorphous fraction decreases from 80 to 20% as the droplet diameter increases from about 200 μm to 900 μm (Fig. 7a). The existence of mixed microstructures over such a wide range of cooling rates is associated with the low crystal growth rate of the Zr-Ti-Cu-Ni-Al alloy.

4. Conclusions

Bulk $Zr_{57}Cu_{20}Al_{10}Ni_8Ti_5$ amorphous ingots can be prepared by melting and freezing in an arc furnace. The low crystal growth rate of this alloy is a contributing factor to its high GFA because it limits the development of the crystals formed at the container wall or from heterogeneous nuclei. ZrO_2 and SiO_2 reduce the GFA due to their role as heterogeneous nucleation agents. The GFA decreases with increasing the amount of the oxides. However, superheating of the melt eliminates

some effects of the oxides. Partially amorphous ingots can still be formed by melting and freezing the alloys in an arc furnace even with addition of 0.2 wt % ZrO_2 or SiO_2. Different types of heterogeneous agents result in different solidification microstructures due to differences in the nucleation rate and nucleation temperature.

Acknowledgements

The authors would like to express their thanks G. P. Görler for the DSC measurement. L. Q. Xing is grateful to the Alexander-von-Humboldt Foundation for financial support.

References

1. D. M. HERLACH, *Mater. Sci. Eng. R* **12** (1994) 177.
2. CLAUDIO S. KIMINAMI, *ibid.* **97** (1988) 195.
3. H. W. KUI, *Appl. Phys. Lett.* **62** (1993) 1224.
4. L. BATTEZZATI, C. ANTONIONE and G. RIONTINO, *J. Non-Crystall. Solids* **89** (1987) 114.
5. A. J. DREHMAN, A. L. GREER and D. TURNBULL, *Appl. Phys. Lett.* **41** (1982) 716.
6. H. W. KUI, A. L. GREER and D. TURNBULL, *ibid.* **45** (1984) 615.
7. Y. HE, R. B. SCHWARZ and J. I. ARCHULETA, *ibid.* **69** (1996) 1861.
8. L. Q. XING, D. Q. ZHAO, X. C. CHEN and X. S. CHEN, *Mater. Sci. Eng.* **A157** (1992) 211.
9. F. GILLESSEN and D. M. HERLACH, *ibid.* **97** (1988) 147.
10. Y. J. KIM, R. BUSCH, W. L. JOHNSON, A. J. RULISON and W. K. RHIM, *Appl. Phys. Lett.* **65** (1994) 2136.
11. A. INOUE, T. ZHANG, N. NISHIYAMA, K. OHBA and T. MASUMOTO, *Mater. Trans. JIM* **34** (1993) 1234.
12. A. PEKER and W. L. JOHNSON, *Mater. Sci. Eng. A* **179** (1994) 173.
13. L. Q. XING, P. OCHIN, M. HARMELIN, F. FAUDOT and J. BIGOT, *J. Non-Crystall. Solids* **205/207** (1996) 597.
14. L. Q. XING, P. OCHIN, M. HARMELIN, F. FAUDOT, J. BIGOT and J.-P. CHEVALIER, *Mater. Sci. Eng. A* **220** (1996) 155.
15. X. H. LIN, W. L. JOHNSON and W. K. RHIM, *Mater. Trans. JIM* **38** (1997) 473.
16. L. Q. XING, G. P. GÖRLER and D.M. HERLACH, *Mater. Sci. Eng. A* **226/228** (1997) 429.

Received 5 February
and accepted 30 November 1998